
Understanding the Power of Persistence Pairing via Permutation Test

Anonymous Author(s)

Affiliation

Address

email

Abstract

1 Recently many efforts have been made to incorporate persistence diagrams, one of
2 major tools in topological data analysis (TDA), into machine learning pipelines.
3 To better understand the power and limitation of persistence diagrams, we carry
4 out a range of experiments on both graph data and shape data, aiming to decouple
5 and inspect the effects of different factors involved. To this end, we also propose
6 the so-called *permutation test*¹ for persistence diagrams to delineate critical values
7 and pairings of critical values. For graph classification tasks, we note that while
8 persistence pairing yields consistent improvement over various benchmark datasets,
9 it appears that for various filtration functions tested, most discriminative power
10 comes from critical values. For shape segmentation and classification, however,
11 we note that persistence pairing shows significant power on most of the benchmark
12 datasets, and improves over both summaries based on merely critical values, and
13 those based on permutation tests. Our results help provide insights on when
14 persistence diagram based summaries could be more suitable.

15 1 Introduction

16 Topological data analysis (TDA) is an emerging field that aims to characterize the shape of low and
17 high dimensional data via methods stemming from algebraic topology. One of the major tools of TDA
18 is persistence diagrams (PDs). In recent years, many efforts have been made to utilize PDs as features
19 for downstream machine learning tasks, such as material science [4], signal analysis [27], cellular
20 data [6] and shape recognition [23]. However, the geometry of the PD does not lend itself easily to
21 well-adopted classifiers due to the lack of Hilbert structure.

22 To handle this issue, a natural way is to apply vectorization [3, 10, 11, 17] or kernelization [9, 28]
23 to PDs, i.e., embedding PDs either to a Euclidean space \mathbb{R}^d or a reproducing kernel Hilbert space
24 (RKHS) associated with certain kernels. However, these approaches still have limitations. First, it
25 has been shown that finite-dimension embedding can miss information about PDs [7]. Second, the
26 time of computing a kernel is quadratic in the number of PDs, which is prohibitive for large scale
27 applications. Third, choosing right vectorization/kernelization and its associated hyper-parameters is
28 not straightforward and usually requires multiple rounds of trial and error.

29 Due to these extra complexities, one may wonder whether the benefits of using PDs outweigh the
30 extra cost. Specifically, PDs have two major components: 1) filtration function and 2) persistence
31 pairing (decomposition of persistence module). In this paper, we ask a simple yet fundamental
32 question: *How much extra power can persistence pairing bring in?*

¹The term shall not be confused with the permutation test in the statistical hypothesis testing.

33 In this work, we propose a simple sanity check named “permutation test” that can shed light on the
34 power of persistence diagram. Specifically, we permute the persistence points in such a way that only
35 coordinates of PDs remain the same but the original pairing is completely destroyed. These fake PDs
36 have the same form as the original PDs and therefore the same kernels for true diagrams can also
37 be applied to fake ones. We use these fake diagrams as the input for various tasks and check their
38 effectiveness. As we will see, this simple trick brings various insights on the use of PDs for different
39 problems.

40 **Our Contributions.** To the best of our knowledge, our paper is the first work systematically
41 quantifying (empirically) the power of persistence pairing for various applications. Specifically, our
42 contributions are the following.

- 43 • We propose the permutation test for PDs that decouples the statistics of the critical values
44 of filtration function and the persistence pairing. Using the proposed permutation test, we
45 find that in graph classification, even fake diagrams perform quite well compared to original
46 PDs. We believe this is due to the noisy nature of graph datasets (PDs are not stable against
47 random insertion and deletion of edges). As a byproduct of our extensive experiments, we
48 also provide some rules of thumb for using PDs in graph classification.
- 49 • For shape segmentation and classification, we find the power of persistence pairing depends
50 on the particular featurization chosen. With the right choice of featurization, utilizing
51 persistence pairing brings in significant improvement. Intuitively, we think that the shape
52 models have more prominent geometric features in them, which are effectively captured by
53 PDs. In contrast, PDs seem to be less effective at capturing features for graphs, partly due
54 to the choice of descriptor functions as well as the nature of noise in graph (e.g., random
55 insertions) which makes PDs less stable.

56 2 Experiment

57 2.1 Setup

58 On a high level, we use PDs obtained from different filtration functions as features. Depending on
59 the task, we choose a proper featurization method (we use kernel methods when possible since they
60 tend to perform better, but for large scale applications, computing kernels is not feasible so we use
61 vector methods), followed by SVM for final classification. We maintain the same experiment settings
62 for original PDs and permuted ones. For a comprehensive evaluation, we perform experiments
63 on various tasks (graph classification, shape segmentation, and object classification) and diverse
64 datatypes including social networks, molecules/proteins, and shapes of different categories.

65 We test degree (deg), Ricci Curvature [24] (Ricci), closeness centrality (cc) and square of Fiedler
66 vector (the eigenvector corresponding to the second smallest eigenvalue of graph Laplacian, denoted
67 as Fiedler-s) for graph classification. On shape datasets, we use geodesic distance as filtration function
68 for shape segmentation and closeness centrality for shape classification. We use Dionysus² to compute
69 PDs and sklearn_tda³ for kernel computation. See details about kernels and datasets at appendix A.2.

70 2.2 Permutation Test and Baselines

71 In this section, we introduce permutation test that aims to preserve statistics of filtration function
72 but destroy the persistence pairing of critical values of the filtration function. For a diagram P of
73 n persistence points $P = \{p_1, p_2, \dots, p_n\}$, denote the coordinates of point p_i by (x_i, y_i) . Take the
74 multiset $P_{multiset} = \{x_1, y_1, x_2, y_2, \dots, x_n, y_n\}$ as input. We then randomly sample two values without
75 replacement from $P_{multiset}$ as the coordinates of the persistence point in the fake diagram. Repeat the
76 same procedure n times and get a fake diagram called P_{fake} of size n .

77 To better quantify the power of persistence pairing, we also introduce two baselines. **Pervec** (vector
78 obtained from coordinates of points in the permuted diagram) is a histogram vector of the coordinates
79 of PD, i.e., the histogram of P . **Filvec** is a histogram vector of all the filtration function values on
80 the graph. The length of Pervec and Filvec is a hyper-parameter chosen from $\{100, 200, 300\}$ by
81 cross-validation.

²<http://mrzv.org/software/dionysus2/>

³https://github.com/MathieuCarriere/sklearn_tda

82 3 Permutation Test for Graphs

83 In this section, we perform graph classification on common benchmark datasets
 84 with different filtration functions and featurizations. Through extensive exper-
 85 iments (see full table on synthetic and real graphs at appendix A.3), we draw
 86 the following conclusions.

87 **Choice of the Filtration Function.** The choice of filtration function clearly
 88 matters. For datasets such as using Ricci curvature as the filtration function
 89 yields the best accuracy as opposed to other filtration functions.

90 If we fix method to be Sliced Wasserstein kernel, for graphs like IMDB-B (69.5
 91 for degree vs. 69.2 for Ricci) and IMDB-M (43.1 vs. 43.7), PROTEINS (73.6
 92 vs. 73.8), D&D (76.1 vs. 76.9), even degree performs as well as Ricci. This is
 93 consistent with the findings in the paper [5] where it is shown simple statistics
 94 based on node degree can perform on par with the state of the art. This raises
 95 the concern that the current benchmark datasets might be limited in evaluating
 96 different methods.

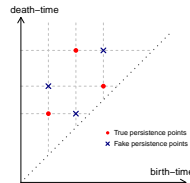


Figure 1: Visualize true and fake diagrams.

graph	BZR	COX2	D&D	DHFR	FRANK	IMDB-B	IMDB-M	NCI1	PROTEIN	PTC	REDDIT 5K
sw w/ Ext_1^-	86.6	80.3	76.2	81.9	70.8	66.2	42.6	77.1	72.7	58.8	53.1
sw w/ Ext_1^-	88.4	80.5	76.9	82.8	72.0	69.5	45.7	77.8	74.0	58.7	54.1
pervec w/ Ext_1^-	85.4	81.6	74.4	80.8	70.1	65.7	42.7	74.4	70.9	59.3	49.5
pervec w/ Ext_1^-	87.6	81.6	77.4	80.0	70.8	67.1	42.9	74.3	72.6	59.3	49.7
Perslay	87.2	81.6	-	81.8	70.7	70.9	48.7	72.8	74.8	-	56.6
WKPI-kM	-	-	82.0	-	-	70.7	46.4	87.5	78.5	62.7	59.1
WKPI-kC	-	-	80.3	-	-	75.1	49.5	84.5	75.2	68.1	59.5

Table 1: Fix featurization as sw and look at the whether adding Ext_1^- in the PDs helps. The accuracy takes the maximum over different filtration function.

97 **Sliced Wasserstein Kernel + Ricci is Powerful.** Choosing the best accuracy for sw among different
 98 filtrations yields decent performance. COX2: 80.5 (best accuracy when using sw) vs. 82.0 (best
 99 accuracy among all filtration functions and featurizations for a single dataset). BZR: 88.4 vs. 88.4. DD:
 100 76.9 vs. 77.4. DHFR: 82.8 vs. 82.8. FRANKENSTEIN: 72.0 vs. 72.3. IMDB-B: 69.2 vs. 69.5. IMDB-M:
 101 45.2 vs. 46.5. NCI1: 77.8 vs. 77.8. PROTEINS: 73.8 vs. 74.0. REDDIT 5K: 54.1 vs. 54.1.

102 As a corollary, to achieve good performance for graph classification, a rule of thumb is to use Ricci
 103 curvature as filtration plus Sliced Wasserstein kernel.

104 **Permutation Test.** Looking at the mean accuracies over four different filtration functions, sw
 105 performs better than sw-p/pervec/filvec, although the amount of improvement depends on the dataset.
 106 For BZR, DHFR, FRANKENSTEIN, IMDB-B, NCI1, PROTEIN, REDDIT 5K sw is better than filvec, pervec,
 107 and sw-p. For COX2, dd, sw is no better than the best of filvec/pervec/sw-p, but the gap (0.2 for COX2
 108 and 1.05 for DD) is small.

109 Pervec and filvec are used as baselines. The performance of pervec, filvec and sw-p is expected to be
 110 close to each other since none of them is using persistence pairing. This is indeed the case. The best
 111 of pervec and filvec is close to sw-p for all the graphs. (The difference is less than 2.5 percent.) Note
 112 hyper-parameter choice for pervec/filvec and sw-p will also result in different performance. After
 113 all, the input for pervec/filvec are vectors while for sw-p the input is fake PDs. We believe that the
 114 difference between pervec, filvec and sw-p is reasonable, and the conclusion that most discriminative
 115 power comes from function values is robust.

116 **Learning for PDs.** We compare the accuracy obtained from sw + best filtration function with
 117 Perslay/WKPI where learning is involved. As shown in Table 1, our method is comparable with
 118 Perslay. We conjecture replacing original filtration (based on heat kernel signature) used in Perslay
 119 with Ricci curvature may improve its performance for some datasets. WKPI (WKPI-kM and WKPI-
 120 kC differs in how they initialize weights.) learns the weights of different points in diagrams, which
 121 results in much better performance. This confirms the belief that to fully utilize the power of PDs, a
 122 proper weighting scheme is crucial.

123 **The Effect of Adding Loops.** We analyze the effect of adding loops (Ext_1^-) in extended PDs for
 124 graph classification. Since extended PDs capture loops in graphs with respect to the filtration function,

125 the hope is that adding Ext_1^- in the PD will make it more discriminative. But one can perhaps argue
 126 the improvement may come from the coordinate values of extended PDs, so we fix featurization as
 127 pervec (as opposed to sw) to see the difference. Table 1 shows that adding coordinates of extended
 128 PDs increase the accuracy, no matter whether we utilize pairing (sw) or not (pervec).

129 4 Permutation Test for Shapes

130 We now perform permutation test on the problem of supervised 3D shape segmentation and object
 131 classification (see appendix A.4 due to space limitation). As we will see, the choice of permuting
 132 diagrams makes a much bigger difference here.

133 For each vertex x , we use the geodesic distance (distance to x) as the filtration function and compute
 134 the super-level 0-PDs as features. We convert PDs into feature vectors via either persistence landscape
 135 [3] or persistence image [1] and use SVM [25] as our classifier.

136 We use Princeton shape benchmark as dataset. This benchmark contains several different ground
 137 truth segmentations for each shape. For each shape in the training set, we use the same ground truth
 138 segmentation as [18]. For each category, we use 50% data for training and the rest for testing. The
 139 results are shown in Table 6, from which we draw following conclusions.

140 The effects of permutation test clearly depend on the vectorization selected. For Persistence Landscape
 141 (PL), there are some categories (such as cup, glasses, vase...) where permuting PDs yields better
 142 results than the original diagrams. We find corresponding diagrams for those categories all have very
 143 few persistence points (less than 2) far away from the diagonal on average. See diagram statistics in
 144 the appendix. In the formulation of persistence landscape, points close to diagonal are treated less
 145 important and thus play a less important role in final shape segmentation. In contrast, permuting PDs
 146 will “pull” those points away from diagonal with high probability and make them more important
 147 under PL’s framework, therefore explaining the fact that permuting diagrams coupled with PL yields
 148 better results for those categories.

149 In contrast, Persistence Image (PI) takes a very
 150 different way to vectorize PDs . In particular,
 151 PI assigns a weight for each point and points
 152 near diagonal are not necessarily assigned small
 153 weight. We use the same weight (proportional
 154 to death time) as in the original paper. It turns
 155 out that 1) permuting PDs for PI always gives
 156 worse result except for categories bearing and
 157 bust where a very small gap exists and 2) PI
 158 yields better results on all shapes compared to
 159 PL. Interestingly, given that PL gives smaller
 160 weights to points closer to the diagonal, while
 161 PI does not necessarily do (as in this experiments), we think this suggests that while PD can identify
 162 “features” of input shapes in a canonical way, the importance of these features (especially in terms
 163 of the tasks they are used for) may not be consistent with their persistence. This point has been
 164 made earlier in [1, 21, 34], which allow assigning different weights to persistence points. In our case,
 165 permutation test is proved to be a handy trick that can be applied to quickly test if the downstream
 166 featurization is effective.

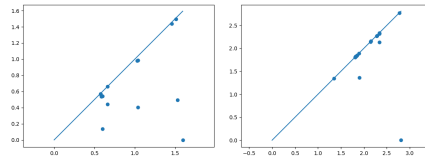


Figure 2: Two corresponding diagrams for Human and Cup. On average, diagrams in Human/Cup has 4.4/1.5 points away from diagonal.

167 5 Conclusion and Future Work

168 By introducing permutation test on PDs , we find persistence pairing is crucial for shape datasets. For
 169 graph datasets, although the small (yet consistent) improvements pairing brings may be unexpected
 170 and unsatisfying, we interpret this due to the challenging nature of graph classification and dataset
 171 problem. In the future, we are interested in understanding the discriminative power of PDs in a
 172 principle way. We believe developing a connection between the structure of persistence module
 173 (persistence pairing) and generalization error is important for the application of PDs in machine
 174 learning.

References

- 175
- 176 [1] Henry Adams, Tegan Emerson, Michael Kirby, Rachel Neville, Chris Peterson, Patrick Shipman,
177 Sofya Chepushtanova, Eric Hanson, Francis Motta, and Lori Ziegelmeier. Persistence images: A
178 stable vector representation of persistent homology. *The Journal of Machine Learning Research*,
179 18(1):218–252, 2017.
- 180 [2] Karsten M Borgwardt, Cheng Soon Ong, Stefan Schönauer, SVN Vishwanathan, Alex J
181 Smola, and Hans-Peter Kriegel. Protein function prediction via graph kernels. *Bioinformatics*,
182 21(suppl_1):i47–i56, 2005.
- 183 [3] Peter Bubenik. Statistical topological data analysis using persistence landscapes. *The Journal*
184 *of Machine Learning Research*, 16(1):77–102, 2015.
- 185 [4] Mickaël Buchet, Yasuaki Hiraoka, and Ippei Obayashi. Persistent homology and materials
186 informatics. In *Nanoinformatics*, pages 75–95. Springer, Singapore, 2018.
- 187 [5] Chen Cai and Yusu Wang. A simple yet effective baseline for non-attribute graph classification.
188 *arXiv preprint arXiv:1811.03508*, 2018.
- 189 [6] Pablo G Cámara. Topological methods for genomics: Present and future directions. *Current*
190 *opinion in systems biology*, 1:95–101, 2017.
- 191 [7] Mathieu Carriere and Ulrich Bauer. On the metric distortion of embedding persistence diagrams
192 into separable hilbert spaces. *arXiv preprint arXiv:1806.06924*, 2018.
- 193 [8] Mathieu Carriere, Frederic Chazal, Yuichi Ike, ThÃ©o Lacombe, Martin Royer, and Yuhei
194 Umeda. Perslay: A simple and versatile neural network layer for persistence diagrams. *arXiv*
195 *preprint arXiv:1904.09378*, 2019.
- 196 [9] Mathieu Carriere, Marco Cuturi, and Steve Oudot. Sliced wasserstein kernel for persistence
197 diagrams. *arXiv preprint arXiv:1706.03358*, 2017.
- 198 [10] Mathieu Carrière, Steve Y Oudot, and Maks Ovsjanikov. Stable topological signatures for
199 points on 3d shapes. In *Computer Graphics Forum*, volume 34, pages 1–12. Wiley Online
200 Library, 2015.
- 201 [11] Frédéric Chazal, Brittany Terese Fasy, Fabrizio Lecci, Alessandro Rinaldo, and Larry Wasser-
202 man. Stochastic convergence of persistence landscapes and silhouettes. In *Proceedings of the*
203 *thirtieth annual symposium on Computational geometry*, page 474. ACM, 2014.
- 204 [12] Xiaobai Chen, Aleksey Golovinskiy, and Thomas Funkhouser. A benchmark for 3d mesh
205 segmentation. In *Acm transactions on graphics (tog)*, volume 28, page 73. ACM, 2009.
- 206 [13] Paul D Dobson and Andrew J Doig. Distinguishing enzyme structures from non-enzymes
207 without alignments. *Journal of molecular biology*, 330(4):771–783, 2003.
- 208 [14] Herbert Edelsbrunner and John Harer. *Computational topology: an introduction*. American
209 Mathematical Soc., 2010.
- 210 [15] Christoph Helma, Ross D. King, Stefan Kramer, and Ashwin Srinivasan. The predictive
211 toxicology challenge 2000–2001. *Bioinformatics*, 17(1):107–108, 2001.
- 212 [16] Christoph Hofer, Roland Kwitt, Marc Niethammer, and Andreas Uhl. Deep learning with
213 topological signatures. In *Advances in Neural Information Processing Systems*, pages 1634–
214 1644, 2017.
- 215 [17] Sara Kališnik. Tropical coordinates on the space of persistence barcodes. *Foundations of*
216 *Computational Mathematics*, 19(1):101–129, 2019.
- 217 [18] Evangelos Kalogerakis, Aaron Hertzmann, and Karan Singh. Learning 3d mesh segmentation
218 and labeling. In *ACM Transactions on Graphics (TOG)*, volume 29, page 102. ACM, 2010.
- 219 [19] Jeroen Kazius, Ross McGuire, and Roberta Bursi. Derivation and validation of toxicophores for
220 mutagenicity prediction. *Journal of medicinal chemistry*, 48(1):312–320, 2005.
- 221 [20] Nils Kriege and Petra Mutzel. Subgraph matching kernels for attributed graphs. *arXiv preprint*
222 *arXiv:1206.6483*, 2012.
- 223 [21] Genki Kusano, Yasuaki Hiraoka, and Kenji Fukumizu. Persistence weighted gaussian kernel for
224 topological data analysis. In *International Conference on Machine Learning*, pages 2004–2013,
225 2016.

- 226 [22] Tam Le and Makoto Yamada. Persistence fisher kernel: A riemannian manifold kernel for
 227 persistence diagrams. In *Advances in Neural Information Processing Systems*, pages 10007–
 228 10018, 2018.
- 229 [23] Chunyuan Li, Maks Ovsjanikov, and Frederic Chazal. Persistence-based structural recognition.
 230 In *Proceedings of the IEEE Conference on Computer Vision and Pattern Recognition*, pages
 231 1995–2002, 2014.
- 232 [24] Yong Lin, Linyuan Lu, and Shing-Tung Yau. Ricci curvature of graphs. *Tohoku Mathematical*
 233 *Journal, Second Series*, 63(4):605–627, 2011.
- 234 [25] Siyuan Ma and Mikhail Belkin. Diving into the shallows: a computational perspective on
 235 large-scale shallow learning. In *Advances in Neural Information Processing Systems*, pages
 236 3778–3787, 2017.
- 237 [26] Steve Y Oudot. *Persistence theory: from quiver representations to data analysis*, volume 209.
 238 American Mathematical Society Providence, RI, 2015.
- 239 [27] Jose A Perea and John Harer. Sliding windows and persistence: An application of topological
 240 methods to signal analysis. *Foundations of Computational Mathematics*, 15(3):799–838, 2015.
- 241 [28] Jan Reininghaus, Stefan Huber, Ulrich Bauer, and Roland Kwitt. A stable multi-scale kernel for
 242 topological machine learning. In *Proceedings of the IEEE conference on computer vision and*
 243 *pattern recognition*, pages 4741–4748, 2015.
- 244 [29] Nino Shervashidze, Pascal Schweitzer, Erik Jan van Leeuwen, Kurt Mehlhorn, and Karsten M
 245 Borgwardt. Weisfeiler-lehman graph kernels. *Journal of Machine Learning Research*,
 246 12(Sep):2539–2561, 2011.
- 247 [30] Jeffrey J Sutherland, Lee A O’Brien, and Donald F Weaver. Spline-fitting with a genetic
 248 algorithm: A method for developing classification structure- activity relationships. *Journal of*
 249 *chemical information and computer sciences*, 43(6):1906–1915, 2003.
- 250 [31] Zhirong Wu, Shuran Song, Aditya Khosla, Fisher Yu, Linguang Zhang, Xiaoou Tang, and
 251 Jianxiong Xiao. 3d shapenets: A deep representation for volumetric shapes. In *Proceedings of*
 252 *the IEEE conference on computer vision and pattern recognition*, pages 1912–1920, 2015.
- 253 [32] Pinar Yanardag and SVN Vishwanathan. Deep graph kernels. In *Proceedings of the 21th*
 254 *ACM SIGKDD International Conference on Knowledge Discovery and Data Mining*, pages
 255 1365–1374. ACM, 2015.
- 256 [33] Manzil Zaheer, Satwik Kottur, Siamak Ravanbakhsh, Barnabas Poczos, Ruslan R Salakhutdinov,
 257 and Alexander J Smola. Deep sets. In *Advances in neural information processing systems*,
 258 pages 3391–3401, 2017.
- 259 [34] Qi Zhao and Yusu Wang. Learning metrics for persistence-based summaries and applications
 260 for graph classification. *arXiv preprint arXiv:1904.12189*, 2019.

261 A Missing details

262 A.1 Background

263 A.1.1 Persistent Homology

264 The definition of our proposed method relies on the so-called persistence diagram induced by a
 265 scalar function. We refer readers to resources such as [14, 26] for formal discussions on persistent
 266 homology and related developments. Below we only provide an intuitive and informal description of
 267 the persistent homology induced by a function under a simple setting. Let $f : X \rightarrow \mathbb{R}$ be a continuous
 268 real-valued function defined on a topological space X . We want to understand the structure of X
 269 from the perspective of f . Specifically, let $X_\alpha := \{x \in X | f(x) < \alpha\}$ denote the sublevel set of X
 270 w.r.t. $\alpha \in \mathbb{R}$. Now as we sweep X bottom-up (top down) by increasing the value, the sequence of
 271 sublevel (superlevel) sets connected by natural inclusion maps gives rise to a filtration of X induced
 272 by f :

$$X_{\alpha_1} \subset X_{\alpha_2} \subset \dots \subset X_{\alpha_m} = X, \alpha_1 < \alpha_2 < \dots < \alpha_m \quad (1)$$

273 We track how the topological features of sublevel sets change in terms of homology classes. In
 274 particular, as α increases, sometimes new topological features are born at time α , that is, new families

275 of homology classes are created in $H_k(X_\alpha)$, the k -th homology group of X . Sometimes, existing
 276 topological features disappear, i.e. some homology classes become trivial in $H_k(X_\beta)$ for some
 277 $\beta > \alpha$. The persistent homology captures such birth and death events, and summarizes them in the
 278 so-called persistence diagram $Dg_k(f)$ (We will call it diagram for short when no ambiguity is raised).
 279 Specifically, $Dg_k(f)$ consists of a set of persistence points $(\alpha, \beta) \in \mathbb{R}^2$, where each (α, β) indicates
 280 a k -th homological feature created at α and killed at β . we also call (α, β) persistence pairing since
 281 it pairs two critical values α and β of the filtration function.

282 In particular, 0 homology is just connected components and can be computed efficiently in $O(\alpha(n)n)$
 283 using union-find data structure where $\alpha(n)$ is an extremely slow-growing inverse Ackermann function.

284 A.1.2 Extended Persistence Homology

285 Ordinary persistence sometimes may be insufficient to encode the topology of an object X . For
 286 example, when X is a graph, the loops persist forever since they are not filled during the sublevel
 287 filtration. Similarly, upfork branching points (w.r.t. the filtration function f) are not captured (while
 288 those pointing downwards are detected), since they do not create connected components in the
 289 sublevel filtration.

290 To address the issues above, extended persistence refines the analysis by also including the super-level
 291 set $X^\alpha = \{x \in X : f(x) \geq \alpha\}$ into the filtration in Eqn (1). Similarly, letting α decrease from
 292 ∞ to $-\infty$ gives a sequence of increasing subsets, for which structural changes can be recorded.
 293 In particular, assuming we have a sequence of reals $\alpha_1 < \alpha_2 < \dots < \alpha_m$ such that $X_{\alpha_1} = \emptyset$
 294 ($X^{\alpha_1} = X$) and $X_{\alpha_m} = X$ ($X^{\alpha_m} = \emptyset$), we consider the following extended sequence:

$$\begin{aligned} \emptyset = X_{\alpha_1} \subseteq X_{\alpha_2} \subseteq \dots \subseteq X_{\alpha_m} = (X; X^{\alpha_m}) & \quad (2) \\ \subseteq (X; X^{\alpha_{m-1}}) \subseteq \dots \subseteq (X; X^{\alpha_2}) \subseteq (X; X^{\alpha_1}) = \emptyset. & \end{aligned}$$

295 where $(A; B)$ denotes a pair of space, and at the homology level, note that the natural map from
 296 $X_{\alpha_m} \rightarrow (X; X^{\alpha_m})$ induces an isomorphism. One can then consider the resulting persistent homology
 297 induced by the above extended sequence, and the resulting PDs are called extended PDs. Persistence
 298 pairings in such diagrams have four types, depending on whether the birth and death happen during
 299 the upward filtration (first line in Eqn (2)) or downward filtration (second line in Eqn (2)). In
 300 the context of graphs, these types are denoted as Ord_0 , Rel_1 , Ext_0^+ and Ext_1^- for downwards
 301 branches, upwards branches, connected components and loops respectively. Overall, we denote
 302 $Dg(G, f) = Ord_0(G, f) \cup Rel_1(G, f) \cup Ext_0^+(G, f) \cup Ext_1^-(G, f)$.

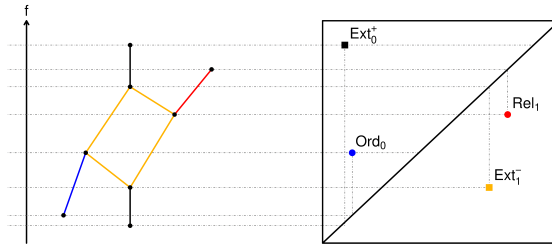


Figure 3: Given the filtration f as height for graph X , the four types of features of graphs and their corresponding persistence points in the extended persistence diagram.

303 A.1.3 PDs for Machine Learning

304 PDs have been proposed as features for machine learning in a series of work (e.g. [1, 11]), starting
 305 from persistence landscapes [3]. We briefly review related methods in this section. The detailed
 306 information can be found in the appendix.

307 **Kernel Method.** Given a set \mathcal{X} (PDs in our case), a function $k : \mathcal{X} \times \mathcal{X} \rightarrow \mathbb{R}$ is called a positive definite
 308 kernel if for all integers n and all families x_1, \dots, x_n of n elements in \mathcal{X} , the matrix $[k(x_i; x_j)]_{i,j}$
 309 itself is positive semi-definite. It is known that kernels generalize scalar products, in the sense that,
 310 given a kernel k , there exists a RKHS \mathcal{H}_k and a feature map $\phi : \mathcal{X} \rightarrow \mathcal{H}_k$ such that $k(x_1, x_2) = \langle \phi(x_1), \phi(x_2) \rangle$.

311 $\phi(x_1), \phi(x_2) \in \mathcal{H}_k$. A kernel k also induces a distance d_k that can be computed as the Hilbert norm
 312 of the difference between two embeddings: $d_k^2(x_1, x_2) = k(x_1, x_1) + k(x_2, x_2) - 2k(x_1, x_2)$.

313 In this paper, we try four common kernels for diagrams, i.e. Persistence Weighted Gaussian Kernel
 314 (pwg) [21], Persistence Scale Space Kernel (pss) [28], Sliced Wasserstein Kernel (sw) [9] and
 315 Persistence Fisher Kernel (pf) [22].

316 **Vector Method.** Another way to use PDs for machine learning is to convert them into vectors. Persis-
 317 tence Landscape (PL) and Persistence Image (PI) are two examples. One advantage of vectorization
 318 over kernelization is that computing kernels takes quadratic time in the number of diagrams while
 319 vectorizing PDs takes only linear time. Thus, we only use vector methods for shape segmentation
 320 where the number of diagrams is roughly 20k-50k.

321 A.1.4 PDs for Graphs

322 For graph classification, [16] is the first work introducing a neural network framework to convert PDs
 323 into feature vectors for graph classification in an end-to-end data-dependent way. Perslay [8] unifies
 324 many existing featurization such as persistence landscape, persistence silhouette [11] and persistence
 325 surface as different instances of a single permutation invariant neural network based on DeepSets [33].
 326 Weighted Persistence Image Kernel [34] (WKPI) is a recently proposed weighted kernel based on
 327 persistence image. WKPI assigns weights for different locations in PDs where weights are learned
 328 from data via gradient descent. Empirically, improved performance over other kernels is shown for
 329 the task of graph classification.

330 A.2 Missing Details at Section 2: Datasets and Choice of Kernels

331 We apply permutation test on diverse data types, whose quantitative summaries are in the appendix.

332 **Graph Datasets:** We perform experiments on common benchmark datasets for graph classifi-
 333 cation. IMDB-B, IMDB-M, REDDIT 5K are composed of social networks. BZR, COX2, DD, DHFR,
 334 FRANKENSTEIN, NCI1, PROTEINS, PTC are graphs from medical or biological applications.

335 **Shape Datasets:** We use Princeton Shape Benchmark [12] for shape segmentation. This benchmark
 336 contains 19 categories of different objects (human, cup, glasses...) with 20 shapes for each category.
 337 For shape classification, we use ModelNet10/ModelNet40 [31] where there are 4899/12,311 CAD
 338 models from 10/40 man-made object categories (bathtub, bed, chair...) respectively.

339 **Choice of Kernels:** We test four kernels for PDs i.e., sw, pss, pwg and pf for different filtration
 340 functions on PROTEINS. As shown in Table 2 in the appendix, the performance of different kernels are
 341 close in terms of accuracy. We prefer Sliced Wasserstein kernel mainly because it is fast ($O(m \log m)$)
 342 as opposed to $O(m^2)$ for pss), easy to tune (search over 5 values for bandwidth as opposed to 45
 343 hyper-parameter combinations for pwg), and still yields decent performance. Note that in this paper
 344 we focus on understanding the extra power persistence pairing brings in, not achieving the state of
 345 the art.

Table 2: Performance of different filtration function and persistence kernels for PROTEINS dataset.

method	cc	deg	Fiedler-s	Ricci	mean
pf	70.3	73.4	72.8	70.6	71.78
pss	74.3	72.5	73.9	73.6	73.58
sw	74.0	73.6	73.5	73.8	73.72
pwg	74.7	72.4	68.4	73.8	72.32

346 A.3 Missing Details at Section 3: Synthetic Graph Data

347 In this section, we perform permutation test on synthetic graph dataset where graphs sampled
 348 from 2 stochastic block models are classified. In particular, denote $sbm(n_1, n_2, p, q)$ as stochastic
 349 block model of two blocks of size n_1 and n_2 , and within each block, the edge probability is p ,
 350 while between blocks, the edge probability is q . We sample 1000 graphs for classification from
 351 $sbm(100, 50, 0.5, 0.1)$ and $sbm(75, 75, 0.4, 0.2)$. This is a simple classification problem and there
 352 are many ways to achieve perfect results.

353 To make the classification harder, we randomly flip some labels. For example, when label noise
 354 is 0.1, we randomly flip 10% of labels. We are interested in the behaviors of whether to perform
 355 permutation test or not under different label noise levels. As shown in Figure 4, independent from
 356 filtration functions used, applying permutation test has rather small effects on the final performance
 357 for different noise levels.

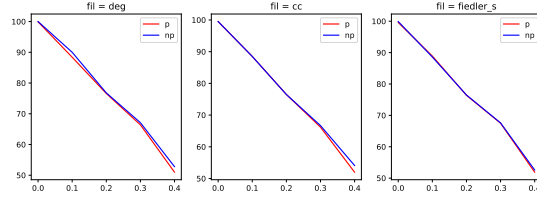


Figure 4: Results on synthetic graph data where the difference between permuting diagram versus not permuting is rather small.

358 A.4 Missing Details at Section 4: 3D Object classification

359 Next, we evaluate our method for shape classification on ModelNet10/ModelNet40. For each shape,
 360 1024 points are uniformly sampled on mesh faces according to face area and normalized into a unit
 361 sphere. We then construct a 8-neighborhood graph from sampled points and use closeness centrality
 362 as our filtration function. For each shape, we use the resulting PDs as the shape representations and
 363 use sw/pf/PI/PL for object classification.

364 Table 5 shows that if we do not utilize persistence pairing, we get very similar results for three methods
 365 (P, Pervec, Filvec), which are much worse than result using PDs (NP), regardless of featurizations. A
 366 detailed performance breakdown on ModelNet 10 is also shown in Table 4 where permuting diagrams
 367 yields much worse results on all shape categories except dresser.

368 Results both in Table 6 and 5 suggest that persistence pairings are effective and meaningful for 3D
 369 models, which partly could be due to that 3D models tend to have clear geometric features that are
 370 also stable under the typical types of (Hausdorff) noise added to these models.

371 In contrast, persistent homology seems to be less effective at capturing features for graphs: this could
 372 partly be due to the choice of descriptor functions used for graphs are not effective at capturing
 373 features. Another potential reason could be that PDs are more sensitive to the common types of
 374 noise in graphs (random insertions), and hence resulting persistence-based features are less stable
 375 and meaningful.

376 A.5 Analysis of True and Fake Diagrams

377 A.5.1 Separation from True and Fake Diagrams

378 Due to the decent result without using persistence pairing on graph datasets, one may wonder whether
 379 there is any useful structure contained in persistence pairing for graph classification. To better
 380 understand the implications of the permutation test, we try to separate true PDs from fake PDs.

381 For each dataset and filtration function, we compute PDs and generate fake diagrams by applying
 382 permutation test. We compute the Sliced Wasserstein kernel and train SVM to discriminate the true
 383 diagrams from the fake ones. We observe in Table ?? consistently that regardless of the datasets and
 384 filtration functions, we can easily get 85%-100% accuracy. This suggests that true diagrams have
 385 some structure that is very different from fake ones.

386 A.5.2 Confusion Matrix Analysis

387 We also examine the confusion matrix in cases where we need to additionally differentiate true/fake
 388 diagrams. In particular, for each graph G_i with label y_i (assume all labels are represented as positive
 389 numbers), we compute the true PD of each graph and generate a fake diagram. In scenario 1) we
 390 assign both diagrams as same label y_i and in scenario 2), we assign two diagram with different label
 391 y_i and $-y_i$. In other words, in the second scenario, a classifier has to differentiate both true/fake

Table 3: The accuracy obtained from filvec, pervec, sw (Sliced Wasserstein Kernel) and sw-p (with permutation) for different filtration functions and datasets.

graph	method	cc	deg	Fiedler-s	Ricci	mean
BZR	filvec	80.7(0.6)	83.4(0.5)	80.5(0.7)	87.6(0.8)	83.05
	pervec	85.4(0.5)	82.5(0.7)	80.5(0.6)	87.6(0.5)	84.00
	sw	86.2(0.5)	83.4(0.6)	81.0(0.4)	88.4(0.6)	84.75
	sw-p	85.1(0.5)	82.2(0.6)	82.2(0.7)	82.7(0.7)	83.05
COX2	filvec	78.8(0.5)	78.2(0.6)	78.8(0.7)	82.0(0.6)	79.45
	pervec	78.8(0.6)	78.2(0.6)	79.4(0.7)	81.6(0.5)	79.50
	sw	79.9(0.7)	78.6(0.5)	78.2(0.7)	80.5(0.5)	79.30
	sw-p	78.2(0.6)	78.6(0.6)	78.8(0.5)	80.1(0.7)	78.93
DD	filvec	75.0(0.4)	72.5(0.4)	67.0(0.6)	76.8(0.6)	72.82
	pervec	75.1(0.4)	70.5(0.6)	66.4(0.5)	77.4(0.5)	72.35
	sw	76.1(0.6)	76.1(0.5)	71.1(0.5)	76.9(0.5)	75.05
	sw-p	76.7(0.5)	76.0(0.6)	74.3(0.4)	77.4(0.5)	76.10
DHFR	filvec	75.1(0.4)	67.3(0.6)	72.1(0.5)	80.1(0.6)	73.65
	pervec	75.5(0.6)	71.3(0.5)	73.3(0.5)	80.8(0.4)	75.23
	sw	79.0(0.7)	73.4(0.6)	74.7(0.4)	82.8(0.5)	77.48
	sw-p	78.7(0.5)	74.7(0.5)	76.6(0.6)	76.5(0.6)	76.62
FRANK	filvec	65.3(0.2)	66.8(0.3)	62.8(0.3)	72.3(0.2)	66.80
	pervec	65.2(0.2)	65.4(0.2)	63.0(0.3)	70.8(0.2)	66.10
	sw	67.8(0.3)	67.3(0.4)	67.1(0.3)	72.0(0.2)	68.55
	sw-p	65.6(0.2)	66.8(0.3)	65.0(0.2)	69.0(0.3)	66.60
IMDB-B	filvec	66.4(0.5)	64.6(0.6)	60.4(0.6)	65.6(0.6)	64.25
	pervec	65.7(0.5)	67.1(0.6)	63.1(0.6)	63.7(0.5)	64.90
	sw	69.5(0.6)	69.5(0.5)	66.5(0.6)	69.2(0.5)	68.68
	sw-p	66.1(0.5)	67.8(0.5)	65.2(0.7)	67.5(0.5)	66.65
IMDB-M	filvec	46.0(0.3)	46.1(0.3)	43.5(0.4)	46.5(0.3)	45.52
	pervec	42.5(0.3)	42.7(0.3)	42.1(0.3)	42.9(0.3)	42.55
	sw	42.6(0.4)	42.6(0.4)	45.7(0.2)	45.2(0.3)	44.03
	sw-p	42.3(0.3)	42.3(0.3)	45.0(0.3)	42.6(0.2)	43.05
NCI1	filvec	69.3(0.2)	64.7(0.3)	67.0(0.3)	74.3(0.3)	68.82
	pervec	69.7(0.2)	63.4(0.3)	64.2(0.3)	74.4(0.1)	67.93
	sw	74.9(0.2)	67.2(0.2)	72.1(0.2)	77.8(0.3)	73.00
	sw-p	69.9(0.3)	64.9(0.2)	69.3(0.2)	71.1(0.2)	68.80
PRO-TEINS	filvec	72.4(0.4)	68.3(0.4)	71.7(0.3)	71.2(0.4)	70.90
	pervec	72.6(0.4)	69.4(0.4)	71.1(0.4)	70.9(0.3)	71.00
	sw	74.0(0.4)	73.6(0.2)	73.5(0.3)	73.8(0.3)	73.72
	sw-p	73.1(0.3)	72.1(0.3)	72.8(0.3)	73.0(0.2)	72.75
REDDIT 5K	filvec	47.0(0.1)	45.8(0.2)	40.3(0.1)	51.0(0.2)	46.03
	pervec	49.2(0.2)	48.9(0.1)	39.0(0.1)	49.7(0.2)	46.70
	sw	52.6(0.2)	49.1(0.1)	42.5(0.1)	54.1(0.1)	49.58
	sw-p	50.4(0.1)	49.2(0.1)	41.9(0.1)	53.3(0.2)	48.70

Table 4: The performance ($F1$ score) breakdown of using PDs for 3D object classification on ModelNet10.

	mean	bathtub	bed	chair	desk	dresser	monitor	night stand	sofa	table	toilet
# of shapes	-	156	615	989	286	286	565	286	780	492	444
$F1$ score wo/ permutation	57.2	54.1	56.4	76.7	21.2	36.3	64.5	46.8	62.1	54.2	74.0
$F1$ score w/ permutation	44.3	24.3	37.3	63.7	0.0	46.1	44.7	31.2	48.8	16.1	15.2

Table 5: Classification accuracy on ModelNet. Four numbers under NP (no permutation) and P (permutation) are accuracies for sw, pf, PI and PL.

	NP	P	Pervec	Filvec
ModelNet-10	55.2/53.6/53.1/53.2	42.7/42.9/41.5/41.5	43.5	44.5
ModelNet-40	43.4/35.8/35.7/34.2	28.1/27.5/27.1/26.9	28.5	30.1

Table 6: The performance (error) of Persistence Landscape (PL) and Persistence Image (PI) for permuting diagrams (P) and not permuting diagrams (NP).

	PL + NP	PL + P	PI + NP	PI + P
Human	7.2	20.9	3.2	8.2
Cup	8.8	5.3	2.6	3.6
Glasses	2.6	2.4	1.6	2.0
Airplane	9.7	17.6	3.5	10.7
Ant	2.5	5.0	1.6	4.6
Chair	3.7	5.0	1.1	4.3
Octopus	2.8	4.5	1.1	3.8
Table	1.6	1.7	0.3	0.9
Teddy	18.6	16.6	4.0	11.3
Hand	10.8	19.0	1.8	10.3
Plier	3.2	4.9	2.9	4.4
Fish	14.4	10.3	7.7	8.1
Bird	8.4	10.8	3.0	9.4
Armadillo	17.1	39.7	4.6	23.6
Bust	44.0	32.5	16.7	15.9
Mech	23.8	18.3	11.0	13.6
Bearing	13.6	6.7	3.3	2.9
Vase	24.3	16.1	7.0	9.2
Fourleg	13.0	20.7	3.5	11.5

Table 7: The accuracy of separating true PDs from fake ones for different graphs and filtration functions.

	deg	Ricci	cc
IMDB-B	99.8	99.5	99.6
IMDB-M	99.8	99.8	99.7
REDDIT 5K	95.7	87.6	91.7
DD	99.5	99.3	99.6

392 diagrams and diagrams of different types of graphs. We want to know whether scenario 2 will make
 393 problem harder.

394 In particular, we use node degree as filtration function and Sliced Wasserstein kernel. It can be seen
 395 in Table 8 that fake diagrams never get confused with true diagrams. We can recover the confusion
 396 matrix on the left from the matrix on the right by merging true and fake diagrams.

397 B Concepts

398 Due to the space limitation, we list definitions of some concepts needed for the paper in the appendix.
 399 We refer readers to [14, 26] for more details.

Table 8: Confusion matrices obtained from kernel SVM without (left)/with (right) fake PDs on DD. I/II: graph types. T/F: whether PDs used are true or fake.

	I	II		I+T	I+F	II+T	II+F
I	121	22	I+T	65	0	8	0
II	38	55	II+F	0	56	0	14
			I+T	25	0	29	0
			II+F	0	13	0	26

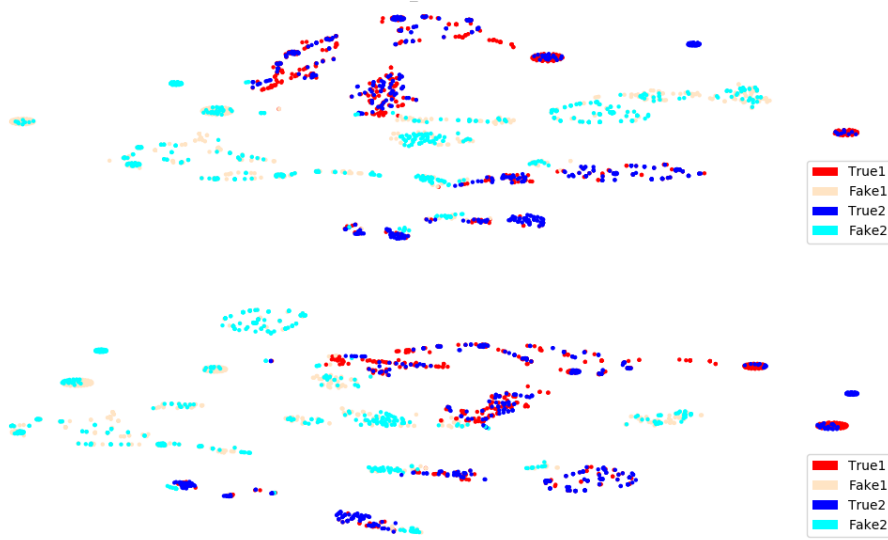


Figure 5: The visualization of true/fake PDs in dark/bright color for IMDB-B. Top: TSNE with kernel distance induced from Sliced Wasserstein kernel. Bottom: TSNE with bottleneck distance (see appendix).

400 B.1 Homology

401 The key concept of homology theory is to study the properties of some object X by means of
 402 (commutative) algebra. In particular, we assign to X a sequence of modules C_0, C_1, \dots which are
 403 connected by homomorphisms $\partial_n : C_n \rightarrow C_{n-1}$ such that $\text{im} \partial_n \subseteq \text{ker} \partial_{n-1}$. A structure of this form is
 404 called a chain complex and by studying its homology groups $H_n = \text{ker} \partial_n / \text{im} \partial_{n+1}$ we can derive
 405 properties of X .

406 B.2 Bottleneck Distance

407 Given two PDs D_1 and D_2 , let $\Gamma : D_1 \supseteq A \rightarrow B \subseteq D_2$ be a partial bijection between D_1 and
 408 D_2 . Then for any point $x \in A$, the p -cost of x is defined as $c_p(x) = \|x - \Gamma(x)\|_\infty^p$ and for
 409 $y \in (D_1 \cup D_2) \setminus (A \cup B)$, the p -cost of y is defined as $c'_p(y) = \|y - \pi_\Delta(y)\|_\infty^p$, where π_Δ the
 410 projection onto the diagonal $\Delta = \{(x, x) : x \in \mathbb{R}\}$. The cost of this partial bijection Γ is defined as
 411 $c_p(\Gamma) = \left(\sum_x c_p(x) + \sum_y c'_p(y) \right)^{1/p}$. Finally, define the p -th diagram distance d_p as the cost of the
 412 best partial bijection:

$$d_p(D_1, D_2) = \inf_{\Gamma} c_p(\Gamma), \quad (3)$$

413 where Γ ranges over all partial bijections between D_1 and D_2 . In the particular case when $p = \infty$,
 414 the cost of Γ is therefore $c(\Gamma) = \max\{\max_x c_1(x) + \max_y c'_1(y)\}$. The corresponding distance
 415 d_∞ is often called the bottleneck distance between diagrams D_1 and D_2 .

416 C Diagram Statistics

417 We list diagram statistics for the shape segmentation task in Table 9. Ave # of PD points (first row)
 418 stands for the average number of persistence points in the diagram for a shape category. A persistence
 419 point is considered as near diagonal if its lifetime is less than one-tenth of the lifetime of the furthest
 420 point in the same diagram.

421 As we can see in Table 9, most persistence points for mech, bust, cup, bearing, glasses, fish, vase,
 422 teddy are concentrated near diagonal. Those are exactly the same categories on which permuting
 423 diagram yields much better results than not permuting diagrams when PI is used.

Table 9: The diagram statistics for different shape categories in Princeton Shape Benchmark.

Category	Mech	Bust	Cup	Bearing	Glasses	Fish	Vase	Teddy	Bird	Plier	Airplane	Table	Human	Armadillo	Chair	Hand	Fourleg	Octopus	Ant
Ave # of PD points	11	22.8	15.9	16.9	7.5	15.1	15.7	18.3	18	6.6	12.5	16.6	58.2	78.6	18.8	19.7	31.4	14.6	15.9
# of points near diagonal	9.9	21.5	14.4	15.3	5.6	13.2	13.7	15.1	14.3	2.9	8.5	12.3	53.7	74.1	14.1	14.5	25.9	6.7	7.3
Difference	1.1	1.3	1.5	1.6	1.9	1.9	2	3.2	3.6	3.7	4	4.3	4.4	4.6	4.7	5.1	5.4	7.9	8.6

424 D Vector Methods for PDs

425 **Persistence Landscape** [3] is the first proposed vectorization method for PDs to overcome some
 426 undesirable property of the space of PDs, such as lacking a unique Frechet mean. This construction is
 427 mainly intended for statistical computations, enabled by the vector space structure of L_p . Given a PD
 428 $D = \{(b_i, d_i)\}_{i=1}^m$, persistence landscape can be thought of as a sequence of functions $\lambda_k : \mathbb{R} \rightarrow \mathbb{R}$
 429 where $\lambda_k(t) = k$ th largest value of $\min(t - b_i, d_i - t)_+$.

430 **Persistent Image** [1] produces a persistence surface ρ_B from a PD by taking a weighted sum of
 431 Gaussians centered at each point. The vector representation, named by persistence image, is created
 432 by integrating persistence surface over a grid. In particular, they fix a grid in the plane with n pixels
 433 and assign to each the integral of ρ_B over that region.

434 There are at least three parameters involved in the construction of persistence image: 1) a non-negative
 435 weighting function 2) the bandwidth of Gaussian kernel (many other functions can be chosen but
 436 in the original paper only Gaussian is considered) and 3) the resolution of the grid put over the
 437 persistence surface. The authors report that in classification experiments they conducted, the accuracy
 438 is insensitive to the choice of resolution and bandwidth.

439 E Kernels Methods for PDs

440 **Persistence Weighted Gaussian Kernel** [21] essentially utilizes the idea of kernel mean embedding
 441 of distribution, where persistence diagram, treated as a special case of distribution, can be embedded
 442 into RKHS. In particular, Let $K, \rho > 0$ and D_1 and D_2 be two PDs. Let K_ρ be the Gaussian kernel
 443 with parameter $\rho > 0$. Let H_ρ be the RKHS associated to k_ρ .

444 Let $\mu_1 = \sum_{x \in D_1} \arctan(Kpers(x)^p k_\rho(*, x)) \in H_p$ be the kernel mean embedding of D_1 weighted
 445 by the diagonal distances. Let μ_2 be defined similarly. Let $\tau > 0$, the persistence weighted gaussian
 446 kernel K_{pwg} is defined as the gaussian kernel with bandwidth τ on H_p :

$$K_{pwg}(D_1, D_2) = e^{-\frac{\|\mu_1 - \mu_2\|_{H_p}}{2\tau^2}} \quad (4)$$

447 **Persistence Scale Space Kernel** [28] represents persistence diagram as sum of Dirac's delta measure.
 448 The persistence scale space kernel is defined as the scalar product of the solution of the heat diffusion
 449 equation with the persistence diagram as an initial value.

450 The closed form

$$K_{pss}(D_1, D_2) = \frac{1}{8} \sum_{p \in D_1} \sum_{q \in D_2} e^{-\frac{\|p-q\|^2}{8t}} - e^{-\frac{\|p-\bar{q}\|^2}{8t}} \quad (5)$$

451 can be computed exactly in $O(|D_1| * |D_2|)$ time where $\bar{q} = (y, x)$ is the symmetric of $q = (x, y)$
 452 along the diagonal. $|D_1|$ and $|D_2|$ denote the cardinality of the multisets D_1 and D_2

453 **Sliced Wasserstein Kernel** [9] uses Sliced Wasserstein approximation of the Wasserstein distance to
 454 define a new kernel for PDs. Different from previous multiple kernels, it is provable not only *stable*
 455 but also *discriminative* (with a bound depending on the number of points in the PDs) w.r.t. the first
 456 diagram distance w_1^∞ between PDs.

457 In particular, the kernel has the following closed-form:

$$K_{sw}(D_1, D_2) = e^{-\frac{SW(D_1, D_2)}{2\sigma^2}} \quad (6)$$

458 where $SW(D_1, D_2)$, is defined as the sliced Wasserstein distance between PDs.

459 **Persistence Fisher Kernel** [22] differs from slice Wasserstein kernel in the sense that the Wasserstein
 460 geometry is replaced by Fisher information geometry (metric), which induces a negative definite
 461 distance. The form of Persistence fisher kernel is

$$k_{PF}(D_1, D_2) = e^{-td_{FIM}(D_1, D_2)} \quad (7)$$

462 where t is a positive scalar and d_{FIM} is the Fisher information metric.

463 **Weighted Persistence Image Kernel** (WKPI) [34] is recently proposed weighted kernel that is based
 464 on persistence image. In particular, WKPI assigns weight for different location in the diagram where
 465 the weight is learned via gradient descent. The form of WKPI is

$$k_w(PI, PI') = \sum_{s=1}^N w(p_s) e^{-\frac{(PI(s) - PI'(s))^2}{2\sigma^2}} \quad (8)$$

466 where PI, PI' are persistence image, s is the location for each pixel in PI , w is the weight function
 467 that will be learned from data. Note that majority of time to compute WKPI is spent on learning
 468 $w(p_s)$ via stochastic gradient descent.

Table 10: Summary of different kernels for PDs. Here n is the number of diagrams. m is the number of persistence points in the diagram of largest size. M_1 is the number of random Fourier feature used for approximating Gaussian kernel. M_2 is the number of directions for approximating Sliced Wasserstein kernel.

	pss	pwg	sw	pf	wkpi
# of Param	1	3	1	2	2
Exact Comp. Time	$O(m^2n^2)$	$O(m^2n^2)$	$O(m^2 \log(m)n^2)$	$O(m^2n^2)$	-
Approx. Time	-	$O(M_1mn + M_1n^2)$	$O(M_2m \log(m)n^2)$	$O(mn^2)$	-

469 F Hyper-parameters Choice

470 We chose our hyper-parameters by 10-fold cross-validation on training set. We list the specific search
 471 range for all methods below. All experiments are performed on a single

472 *Persistence Landscape*: the number of $\lambda_k(t)$ are chosen from $\{3, 4, 5, 6, 7, 8\}$ and each function
 473 $\lambda_k(t)$ is discretized into $\{50, 100, 200, 300\}$ bins.

474 *Persistence Image*: we use the same weight function (Gaussian) in the original paper, the resolution
 475 chosen from $\{20*20, 30*30\}$, and bandwidth of Gaussian is selected from $\{0.01, 0.1, 1, 10, 100\}$.

476 *Persistence Scale Space Kernel*: the parameter t is chosen from 13 values: $\{0.001, 0.005, 0.01, 0.05,$
 477 $0.1, 0.5, 1, 5, 10, 100, 500, 1000\}$.

478 *Sliced Wasserstein Kernel*: following the original paper [9], we grid search bandwidth from the 5
 479 values: $\{0.01, 0.1, 1, 10, 100\}$ and the number of slices, i.e., M_2 is set to be 10.

480 *Persistence Weighted Gaussian Kernel*: we try all the combinations of 5 values from $\{0.01, 0.1, 1, 10,$
 481 $100\}$ for bandwidth, and 3 values from $\{0.1, 1, 10\}$ for both K and ρ , leading to 45 different sets of
 482 parameters.

483 *Persistence Fisher Kernel*: there are two hyper-parameters t and τ (for smoothing persistence
 484 diagram), both of which are selected from $\{0.01, 0.05, 0.1, 0.5, 1, 5, 10, 50, 100\}$.

485 *Pervec/Filvec*: The length of the vector is chosen from $\{100, 200, 300\}$.

486 *Choice of SVM hyper-parameter:* For kernel SVM, the only hyper-parameter C is selected from
 487 $\{0.01, 1, 10, 100, 1000\}$. For Pervec and Filvec, Gaussian kernel is utilized where the bandwidth is
 488 selected from $\{0.01, 0.1, 1, 10, 100\}$.

489 *Graph Classification:* We follow the standard protocol in graph classification literature, i.e., 10-fold
 490 cross-validations, using 9 folds for training and the rest for testing, and repeat the experiments 10
 491 times. We report the average classification accuracies.

492 G Datasets Description

493 The statistics of the benchmark graph datasets used in the paper are reported in Table 6. Due to space
 494 limitation, we only list the dataset statistics here. We provide detailed dataset description in the data
 495 appendix.

Table 11: Statistics of the benchmark graph datasets.

Datasets	graph #	class #	average_nodes #	average edges #	label #
BZR	405	2	35.75	38.36	+
COX2	467	2	41.22	43.45	+
DD	1178	2	284.32	715.66	+
DHFR	467	2	42.43	44.54	+
FRANKSTEIN	4337	2	16.90	17.88	-
IMDB BINARY	1000	2	19.77	96.53	-
IMDB MULTI	1500	3	13.00	65.94	-
NCI1	4110	2	29.87	32.30	+
PROTEINS	1113	2	39.06	72.82	+
PTC	344	2	14.29	14.69	+
REDDIT 5K	4999	5	508.82	594.87	-

496 G.1 Non-attributed Graph Datasets

497 **IMDB-BINARY** [32] is a movie collaboration dataset that consists of the ego-networks of 1,000
 498 actors/actresses who played roles in movies in IMDB. In each graph, nodes represent actors/actresses,
 499 and there is an edge between them if they appear in the same movie. These graphs are derived from
 500 the Action and Romance genres.

501 **IMDB-MULTI** is generated in a similar way to IMDB-BINARY. The difference is that it is derived
 502 from three genres: Comedy, Romance, and Sci-Fi.

503 **REDDIT-BINARY** consists of graphs corresponding to online discussions on Reddit. In each graph,
 504 nodes represent users, and there is an edge between them if at least one of them responds to the other’s
 505 comment. There are four popular subreddits, namely, IAmA, AskReddit, TrollXChromosomes, and
 506 atheism. IAmA and AskReddit are two question/answer based subreddits, and TrollXChromosomes
 507 and atheism are two discussion-based subreddits. A graph is labeled according to whether it belongs
 508 to a question/answer-based community or a discussion-based community.

509 **REDDIT-MULTI (5K)** is generated in a similar way to REDDIT-BINARY. The difference is that
 510 there are five subreddits involved, namely, worldnews, videos, AdviceAnimals, aww, and mildlyinter-
 511 esting. Graphs are labeled with their corresponding subreddits.

512 G.2 Attributed Graphs

513 **PTC** [15] consists of graph representations of chemical molecules. In each graph, nodes represent
 514 atoms, and edges represent chemical bonds. Graphs are labeled according to carcinogenicity on
 515 rodents, divided into male mice (MM), male rats (MR), female mice (FM), and female rats (FR).

516 **PROTEINS** [2] consist of graph representations of proteins. Nodes represent secondary structure
 517 elements (SSE), and there is an edge if they are neighbors along the amino acid sequence or one of
 518 three nearest neighbors in space. The discrete attributes are SSE types. The continuous attributes are
 519 the 3D length of the SSE. Graphs are labeled according to which EC top-level class they belong to.

520 **DD** [13] consists of graph representations of 1,178 proteins. In each graph, nodes represent amino
 521 acids, and there is an edge if they are less than six Angstroms apart. Graphs are labeled according to
 522 whether they are enzymes or not.

523 **NCI1** [20, 29] consists of graph representations of 4,110 chemical compounds screened for activity
524 against non-small cell lung cancer and ovarian cancer cell lines, respectively.

525 **FRANK** [19] is a chemical molecule dataset that consists of 2,401 mutagens and 1,936 nonmutagens.
526 Originally, nodes are associated with chemical atom symbols.

527 **BZR**, **COX2**, and **DHFR** [30] all are chemical compound datasets. Still, in each graph, nodes
528 represent atoms, and edges represent chemical bonds. The discrete attributes correspond to atom
529 types. The continuous attributes are 3D coordinates.